Key Engineering Materials
ISSN: 1662-9795, Vol. 926, pp 569-579
doi:10.4028/p-3b3cjo

Submitted: 2021-12-05
Revised: 2022-01-13
Accepted: 2022-01-17
Online: 2022-07-22

FEM Modelling of Weld Damage in Continuous Cold Rolling of MIG/MAG Butt-Welded Stainless Steel Strips

DEMOULIN Leyne[1,2a], ZAHAR Zineb[1,2b], EL MEKKAOUI Achraf[1,2c], REIGNIER Arnaud[2d], MOCELLIN Katia[1e], MONTMITONNET Pierre[1f *], LEGER Pierre-Emmanuel[2g]

[1]MINES ParisTech, PSL Research University, Centre de mise en forme des matériaux (CEMEF), CNRS [UMR 7635], CS 10207, 06904 Sophia Antipolis Cedex, France

[2]Aperam Isbergues, Research Center, BP 15, 62330 Isbergues, France

[a]leyne.demoulin@edu.supmeca.fr, [b]zinebzahar.zz@gmail.com, [c]achrafelmekk@gmail.com, [d]Arnaud.reignier@aperam.com, [e]katia.mocellin@mines-paristech.fr, [f]pierre.montmitonnet@mines-paristech.fr, [g]pierreemmanuel.leger@aperam.com

Keywords: Strip rolling, butt-welded strips, FEM modelling.

Abstract. Weld line fracture of butt-welded strips in stainless steel continuous rolling has been studied by numerical simulation using ForgeNxT®. The simulation plan includes weld line geometry as well as weld metal constitutive model parameters. The damage criterion used is the non-dimensional Latham & Cockroft function near the singular points of the weld line. Results are confronted to qualitative observations of fracture frequency and fracture initiation loci on the rolling line. Not surprisingly, the protrusion height of the weld line with respect to the strip top surface is found to be a major factor of risk. A second one pertains to the nature of the alloys used: due to the mushroom-like weld line cross-section geometry, damage at the top surface junction of the base metal and the weld metal becomes critical when the weld metal is harder than the base metal. Finally, on the rolling line investigated, prior to rolling properly speaking, the strip goes through a scale-breaking unit followed by acid pickling to eliminate oxides; the multiple, reverse plastic bending applied there contributes significantly to ductile damage, completing the explanation of why the fracture initiation locus is always found to be the same on the rolling line.

Introduction

A few stainless-steel cold rolling mills are designed as continuous, 2-stand tandem mills, requiring butt-welding of successive strips. This introduces weak points and indeed, breaks are occasionally observed. In response, either the rolling stand must be opened to avoid rolling the weld, resulting in more out-of-gauge metal; or a break may occur, and the mill must be stopped. Both result in extra costs and productivity loss, which justifies a mechanical study of weld damage.

Breaks always occur at 1st stand exit and at a specific location, the top surface singular point between the weld line and the base metal of the upstream strip (Fig. 1). Break frequency depends on rolled alloy, ferritic/austenitic. The purpose of this paper is to unveil the reasons behind this behavior.

Although continuous rolling of carbon and alloyed steels has been in use for decades, there are very few studies in the open scientific literature on the question of the weld line behavior [1]. More abundant are the patents on electric flash butt-welding or Laser butt-welding of plain carbon steel strips for continuous rolling (e.g. [2-3]). Butt-welding may be installed for the continuity of different stages of the cold rolling plant, continuous pickling-rolling, continuous annealing, hot dip galvanizing. The most critical is however when the weld must be plastically deformed in the rolling mill. Documents [1-3] point to the main risk factors: poor alignment of the strip ends due to waviness, excessive height of the weld bead, base metal / weld metal hardness ratio, formation of a weak Heat Affected Zone (HAZ) and of course, depending on the strips to be joined, brittleness of the weld metal. 99.9% reliability is claimed in recent suppliers' brochures [4]. Yet, breaks occur.

Process Description

Welding is the first operation on the line. Hot rolled coils, 2 to 3 mm thick, are butt-welded together for continuity by Metal Inert Gas / Metal Active Gas arc welding (MIG/MAG). Whatever the strip alloy, austenitic or ferritic, an austenitic steel wire is used as the weld metal, for operational simplicity. Strip extremities are sheared, carefully positioned a few mm apart and molten weld metal is poured in the interval. This gives the shape visible in Fig. 1; the "funnel-like" shape inside the welded strip is due to melting of the strip metal in the top surface area by the excess of weld metal which forms the protruding bead. The exact shape of the molten metal zone is therefore not completely controlled and is reproducible in its general features only. Of course, a HAZ forms, with mechanical properties slightly different from the hot rolled metal, but its effect is left for future work.

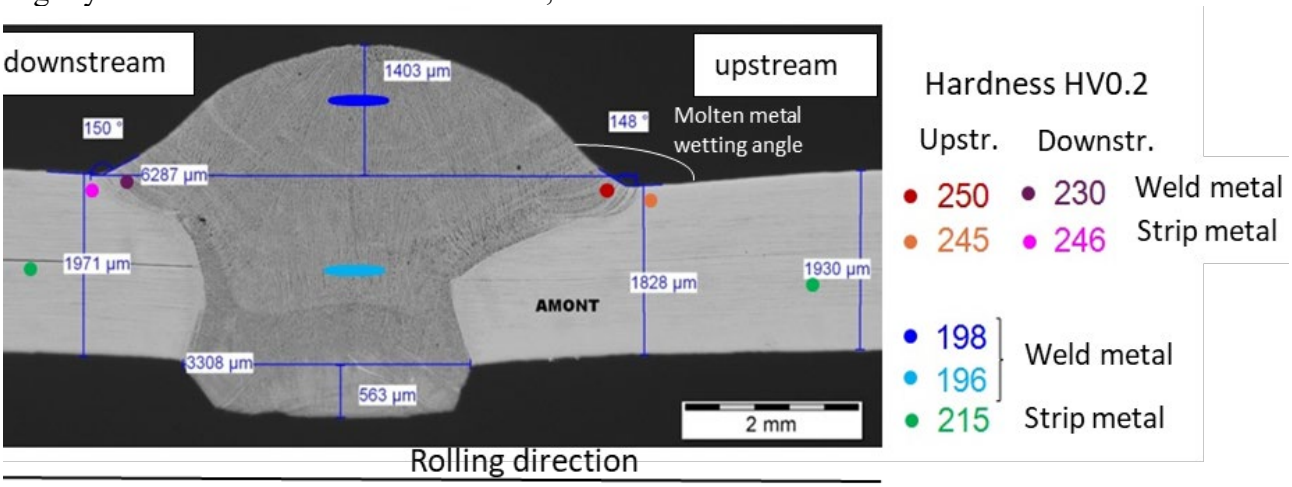

Figure 1: Cross section of a real weld line after the scale-breaker. Strip metal: hot rolled AISI 304L, weld metal: filler wires ER 310 or ER 316LSi.

Following welding and prior to rolling properly speaking, several operations are devoted to oxide removal. It starts with the scale-breaker, followed by two-face shot-blasting which completes oxide fragmentation in order to improve the efficiency of the chemical etching to follow. Rinsing tanks close this part of the line. Of interest here is the scale-breaker, which operates an alternate bending under tension (Fig. 2), resulting in superficial plastic strain. Rollers are idle, the entrainment is provided by the strip tension from the rolling mill. Shot blasting certainly adds further superficial strain and damage but this one should be uniform, so that it will not be dealt with in this paper.

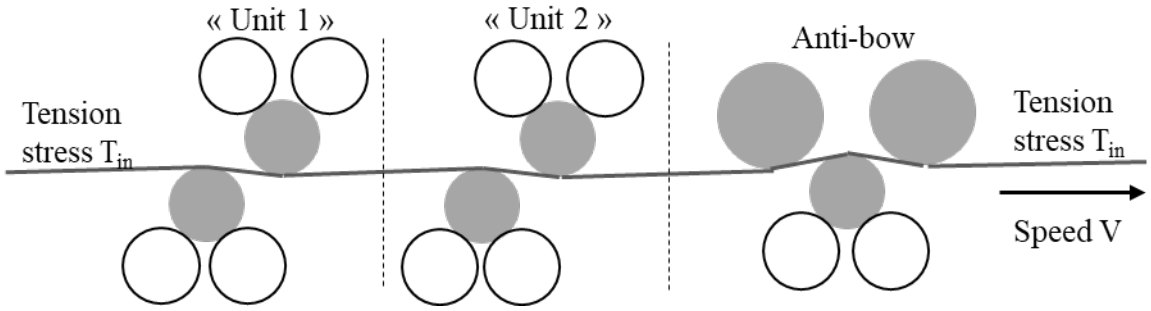

Figure 2: Principle of scale-breaking by plastic bending under strip tension.

Next comes the two-stand rolling mill. Work roll diameter is small (120 mm), the rolling speed is quite low for cold rolling (20 m/min or 0.33 $m.s^{-1}$). Strong strip tensions are applied, the front tension being of the order of twice the back tension. Reductions ~35% per pass are performed under oil lubrication. Only the first stand will be dealt with here as all breaks occur at its exit.

The rest of the line is briefly sketched here for completeness only, as it has nothing to do with weld fracture: continuous annealing, final etching (electrochemical, then chemical), skin pass rolling and roller levelling to optimize strip shape and surface state, and finally coiling.

Fracture characteristics.

Fracture initiation locus. Initiation seems to be always from the top surface, upstream side of the weld line, at least in the few tens of cases investigated occasionally along the years. Fracture propagates mostly along the interface (or in the HAZ), sometimes bifurcates into the base metal (Fig. 3). The interface itself seems not to be a particularly weak zone.

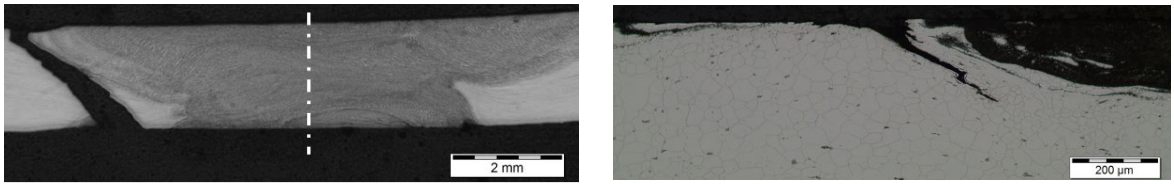

(a) ----------> Rolling direction (RD) (b)

Figure 3: Cross-section micrographs of fractures. (a) austenitic case; (b) ferritic case

Fracture frequency. Quasi-systematic fracture after pass 1 has been found in the past for the ferritic grade, which is welded using an austenitic wire (explaining this is one of the purposes of the work). Therefore, in practice, the mill is systematically opened for the weld line transit, so that no recent observation is available. Experimental fracture observations are therefore mostly on austenitic grades.

Thinning due to bending during scale-breaking. A peculiar observation at the exit of the scale-breaker is a strip thinning of 3-5% all along the strip and 7-10% over the ~5 mm next to the weld line, mainly on the upstream side. This effect can be referred to bending under tension [5,6]. It has been shown in the course of the present study that it does not result in any significant weakness, contrary to the singular points. Its importance lies in the fact that this is a feature which allows checking strip behavior in the scale-breaker.

Design of numerical experiment. Thus, only qualitative information was available, mainly on break frequency and fracture locus: a full quantitative comparison was impossible. A parametric study has therefore been carried out, in which the relative risk of fracture has been estimated using the Latham and Cockroft damage function [7]. The first process parameter is weld line geometry: top and bottom bead protrusion height, molten metal wetting angle. As fracture frequency depends on rolled alloy, the base metal / weld metal hardness ratio has been taken as the second, material parameter.

As a first stage, only damage from the first rolling pass has been considered. It has proved sufficient to explain fracture locus in the case of the ferritic steel. As this was not the case for the austenitic grade, a study of the scale-breaker has been added, showing a quite significant plastic strain and damage. Finally, the two stages, scale-breaker and rolling, have been chained, resulting in a correct prediction of the maximum fracture risk locus.

Numerical Models

ForgeNxT®. All computations were carried out using ForgeNxt® [8], a quasi-static implicit Finite Element Method (FEM) software based on velocity-pressure formulation (v,p). It uses tetrahedron (in 3D) and triangle (in 2D) mini-elements, with linear interpolation of pressure and linear + bubble function interpolation of velocity [9,10]. It offers automatic remeshing. However, neither bending nor rolling result in large distortion; moreover, using remeshing first, some inconsistencies were attributed to the field transfer stage. Remeshing has therefore been disactivated in this study.
The real problem shows some 3D features, mainly:

- weld line is in fact oblique, oriented 5° from the transverse direction.
- The MIG/MAG process uses two torches starting from the drive side and the operators' side and meeting halfway: the bead is generally thicker at strip center.

However, a 2D plane strain approximation has been used here for CPU cost reasons; the thicker central weld bead will be dealt with as a parametric variation instead.

The thermomechanical coupling has not been activated here. Temperature increase is small (low rolling speed) and negligible impact on mechanical properties has been assumed. This could be questioned for unstable austenitic grades due to the sensitivity of martensitic transformation to temperature, but the investigation of this feature is left for future work.

Strip characteristics.

Geometry. Strip thickness is 2.5 mm for ferritic grade AISI 441, 2.15 mm for austenitic grade AISI 304L. As weld bead shape forbids symmetry (Fig. 1 and 4), the whole thickness is meshed. The bead shape and dimensions have been chosen as "averages" of several measured ones – significant variations have been mentioned already.

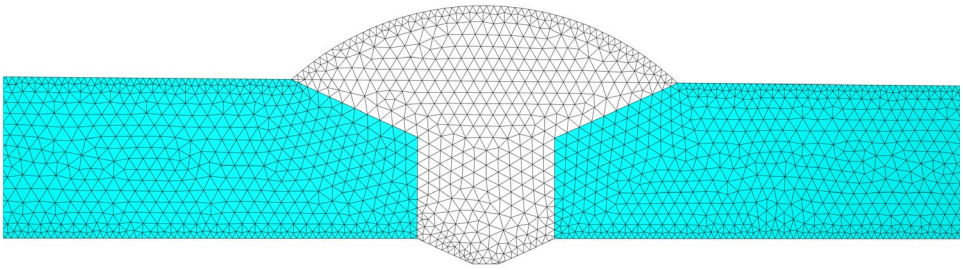

Figure 4: Numerical model, geometry and meshing of the weld line and strip metal.

Meshing. The problem contains singularities (interface, corner points) where a fine mesh is needed. High sensitivity to the mesh has been found indeed. Furthermore, bending induces strain and stress gradients which are essential to capture. In the following therefore, a mesh size of 0.1 mm is used most of the time in the vicinity of the weld, as shown in Fig. 4. As for the bimaterial character, the single domain strategy was kept: a global geometry is meshed, then the area of the weld metal is defined by an inserted contour and its own mechanical properties are activated there. This single domain character means that neither sliding not fracture is allowed along the interface: the former is impossible in practice anyway, the latter will not be modelled explicitly, only the risk estimated through a damage function.

Mechanical properties. Elastic-plastic behavior is assumed. The stress-strain curves based on tension tests performed on the hot rolled metal are shown in Fig. 5 as full lines and represented by Eq.(1) ($\bar{\varepsilon}$ is the equivalent plastic strain and $\bar{\sigma}$ the von Mises stress):

$$\bar{\sigma} = A(1 + k\bar{\varepsilon})^n \tag{1}$$

A key point for the following is that, due to partial martensitic transformation, the strain-hardening capacity of the austenitic grades is much larger than that of the ferritic grades.

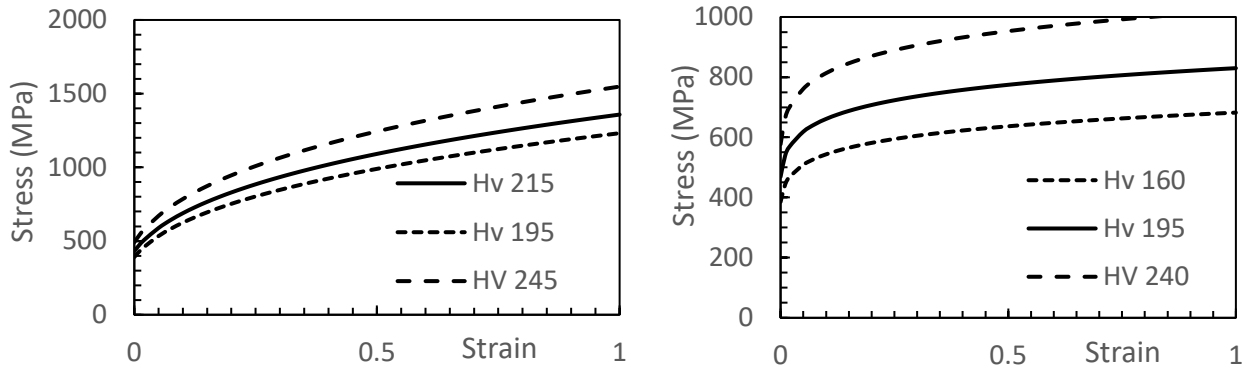

(a) (b)

Figure 5: Stress-strain curves of base metal and weld metal. (a) austenitic grade (304L); (b) ferritic grade (441). Measured curves pictured with full lines, parametric variations with broken lines.

On the weld metal (austenitic), only hardness measurement was possible. The shape of the strain-hardening curve was copied from the base metals by using the hardness ratio. Thus, for the austenitic grade, the strip hardness is 215 HV, the weld metal (ER 310) hardness is 195 HV (see Fig. 1). Just multiplying parameter A by the hardness ratio 195 / 215 results in the curve "Hv 195" in Fig. 5a. It is used in the following for the weld metal, but also in the parametric study on the austenitic strip mechanical properties. For the latter purpose, another curve "Hv 245" has been built in order to vary more widely the strip / weld metal hardness ratio, known to be an important factor in weld line breaks.

The ferritic strip hardness is 195 HV. It is welded with austenitic ER310 as stated before, which has the same initial hardness but work-hardens much more, reaching a state where the weld metal yield stress is above the strip yield stress. This proved decisive for metal flow and damage risk.

Overall, the hardness ratio has been scanned in the interval [0.7-1.4] for the ferritic as well as the austenitic case, in order to include, in both cases, situations with harder strip and others with harder weld metal. Examples of these parametric variations are given in Fig. 5b as dotted lines.

Scale-Breaking unit.

Geometry. The rollers, rigid and idle, are meshed finely to ensure a good geometrical description. In the simulation, their meshes do not rotate but rollers are given a tangential velocity equal to the line velocity. As there is no slip which could dissipate energy, zero friction is assumed for simplicity.

Boundary conditions. The whole scale-breaker is more than 1.5 m long. Modelling it in one stage would require a very long meshed strip coupon leading to unreasonable computing times. This is why it has been split into 3 stages corresponding to the 3 "units" of Fig. 2. Thanks to this, the meshed strip length could be reduced to 800 mm. In each, a back tension is applied on the upstream side, the downstream side is given the line velocity. In each section, a flat strip is positioned between the rollers in the opened position, then the latter are vertically displaced to apply bending before the horizontal pull is applied on the strip. This requires clipping the residual curved length for the next unit. Care has been taken not to disturb the mechanical fields in so doing.

Rolling mill.

Geometry. Again, rolls are modelled as rigid, diameter Φ = 120 mm. Roll mesh does not rotate but it is given a tangential velocity, 20 m/min (0.33 $m.s^{-1}$).

Boundary conditions. A strip length of 30 mm has been found sufficient for the rolling stage modelling. It allows reaching steady state before the weld line is rolled and resuming steady state once it has been rolled. The strip is imposed a purely horizontal movement at exit (zero vertical component) due to the constraint applied by the second stand. But the upstream end is left free to move vertically as it will be shown that significant bending occurs when the weld bead first contacts rolls. The required strip tensions are applied in the horizontal direction.

Friction has been identified by fitting the measured roll load in the steady state (far from weld line): friction factor is equal to 0.3.

Results

Analysis of rolling without prior mechanical history.

General sketch of the weld line behavior. The weld line contacts the upper roll first, the upstream part bends downward so that the root of the weld line, below the bottom strip surface, in turn contacts the lower roll (Fig. 6a). At this stage, the bead has rotated counterclockwise together with the neighboring segments of the strips. The horizontal back tension fights against this movement and puts in tension the angle upstream (i.e. left on the figures) on the bottom surface. This is a local plastic bending which initiates tensile damage even before this point contacts the roll.

The bead forms a temporary obstacle to the penetration as local reduction reaches almost 80%, to be compared to the nominal 35%. But it is entrained, provided sufficiently high friction is ensured. The two gaps just downstream (i.e. right) of the bead, visible in Fig. 6a, form angles of 135° (by design of the root) and 140° ("weld metal wetting angle") which open into flat angles as they progress in the bite *without contact*; this unbending effect initiates tensile damage at these points (Fig. 6b);

beyond closure, they are submitted to compressive stress and further damage is limited, except when crossing steady shear bands which are typical features of strip rolling. Then, the upstream strip metal contacts the lower roll while the weld metal is still in contact with the upper roll, inducing reverse (upward) bending (Fig. 6c). At this stage, the upstream strip is pushed upward while the weld metal of the cap of the bead is pushed downward: this kind of diffuse shear effect initiates damage at the upstream, top surface angle. When the bead has sufficiently progressed into the roll bite for the base metal to form the entry both on the upper and lower roll, the strip becomes flat again (Fig. 6d).

These tail movements may depend on the restraint opposed by the weight and stiffness of the non-modelled, upstream part of the strip. It has been checked that modified upstream boundary conditions, forcing the strip horizontal here also, does not change the results to a significant extent.

Note that a non-dimensional Latham and Cockroft function (LC) has been used here [8]:

$$LC = \int_0^{\bar{\varepsilon}_f} \frac{Max(\sigma_I,0)}{\bar{\sigma}} . d\bar{\varepsilon} \qquad (2)$$

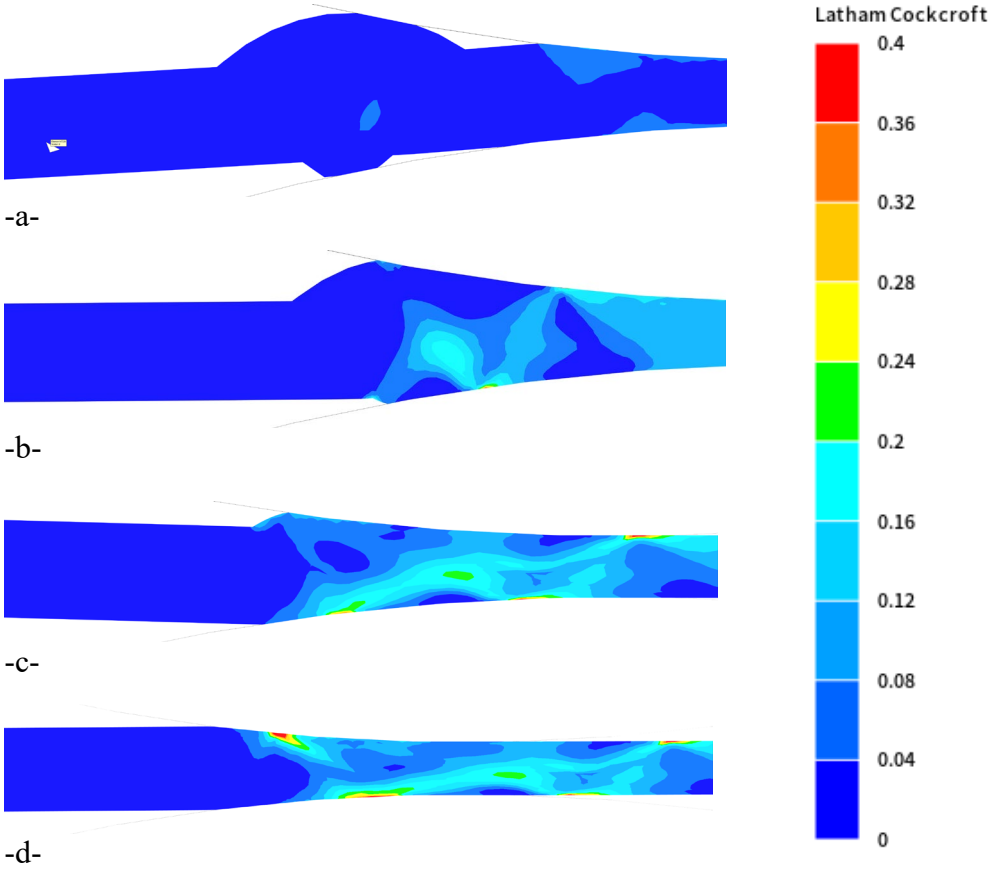

Figure 6: Snake-like creeping of the bead as it enters the roll bite and progresses.

Comparison of different bead heights. As a crucial parameter, bead height has been varied. A height of 2.8 mm has been compared with the nominal 1.4 mm. This corresponds qualitatively to the strip center where the two torches may superimpose their weld metal.

Fig. 7 clearly shows that a higher bead very significantly increases LC damage function value. The maximum jumps from 0.38 to quite high 0.81; the increase is mostly on the upper surface, which makes sense – this is where the excess weld metal is thrust into the interval between strips. This confirms the danger of such excess height; indeed, fractures are often found to initiate at strip center.

Other geometrical features have been investigated (wetting angles, cap and root shapes) but found of secondary importance compared with bead height. Therefore, next action consisted, starting from the same bead, initially 1.4 mm, in erasing its top to 1/3 of the initial height. Fig. 7c confirms a strong decrease of the damage function everywhere, although again the top surface values vary most. The

maximum damage is now on the bottom surface, where the now thicker root weld metal is pushed between the strips. All this suggests a potential remedy. One caveat however: maximum damage is found here at the downstream side of the weld line (i.e. on the right), on the top surface or the bottom surface, whereas experience points to the upstream side (left), top surface. The locus is therefore not predicted correctly. This problem is addressed in the next sections.

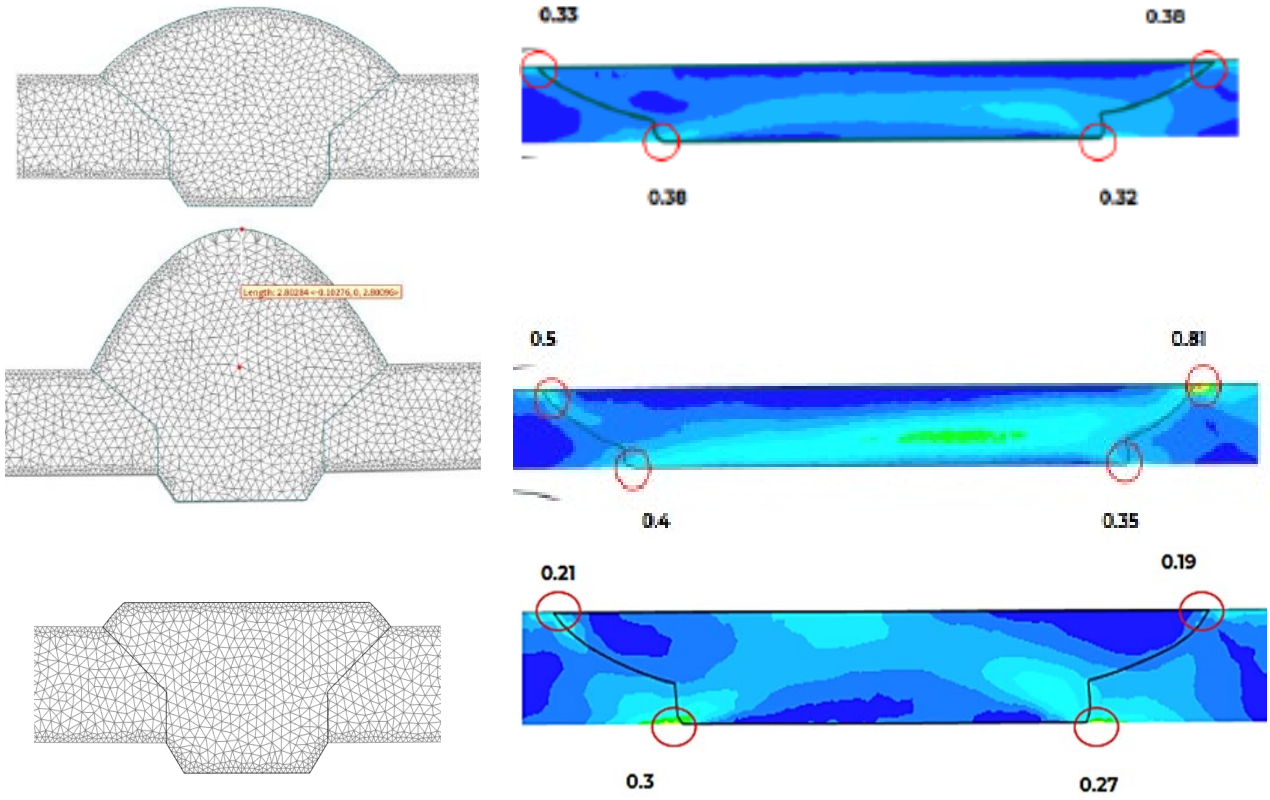

Figure 7: Impact of the bead thickness on the LC map. Austenitic strip and weld metal. Rolling direction (RD) is from left to right.

Effect of the hardness ratio. The austenitic grade is considered again. Playing numerically with the value of A in Eq.(1) makes the weld metal softer / equal in hardness / harder than the base metal. The strain is always large in the center of the weld bead, where the local thickness reduction is largest (Fig. 8, left). For extreme values of Hv_{strip}/Hv_{weld}, oblique shear bands develop along the interface, in the softer of the two alloys. The right part of Fig. 8 shows how, as a consequence, the most damaged point moves from bottom surface upstream to top surface upstream (i.e. left) as the weld metal gets harder and harder, as its V-shaped part just below the top surface "pinches" the base metal below it.

This explains the high frequency of fractures of the ferritic AISI 441 grade. Indeed, it is butt-welded using austenitic ER 310 grade weld metal. In the first few percent of strain, 441 is harder; but beyond ~15% strain, ER 310 weld metal becomes harder. In a 35% thickness reduction pass, the latter situation prevails over 2/3 of the bite length. Indeed, Fig. 9 shows that the maximum damage is found at the correct location, the singular point at the top surface of the upstream strip, near the interface but larger in the strip metal. The reason is again that the underlying strip metal is compressed by the harder weld metal in the triangles above: two shear bands betray this deformation mechanism. This explains why these ferritic strips bonded with austenitic weld metal are more sensitive.

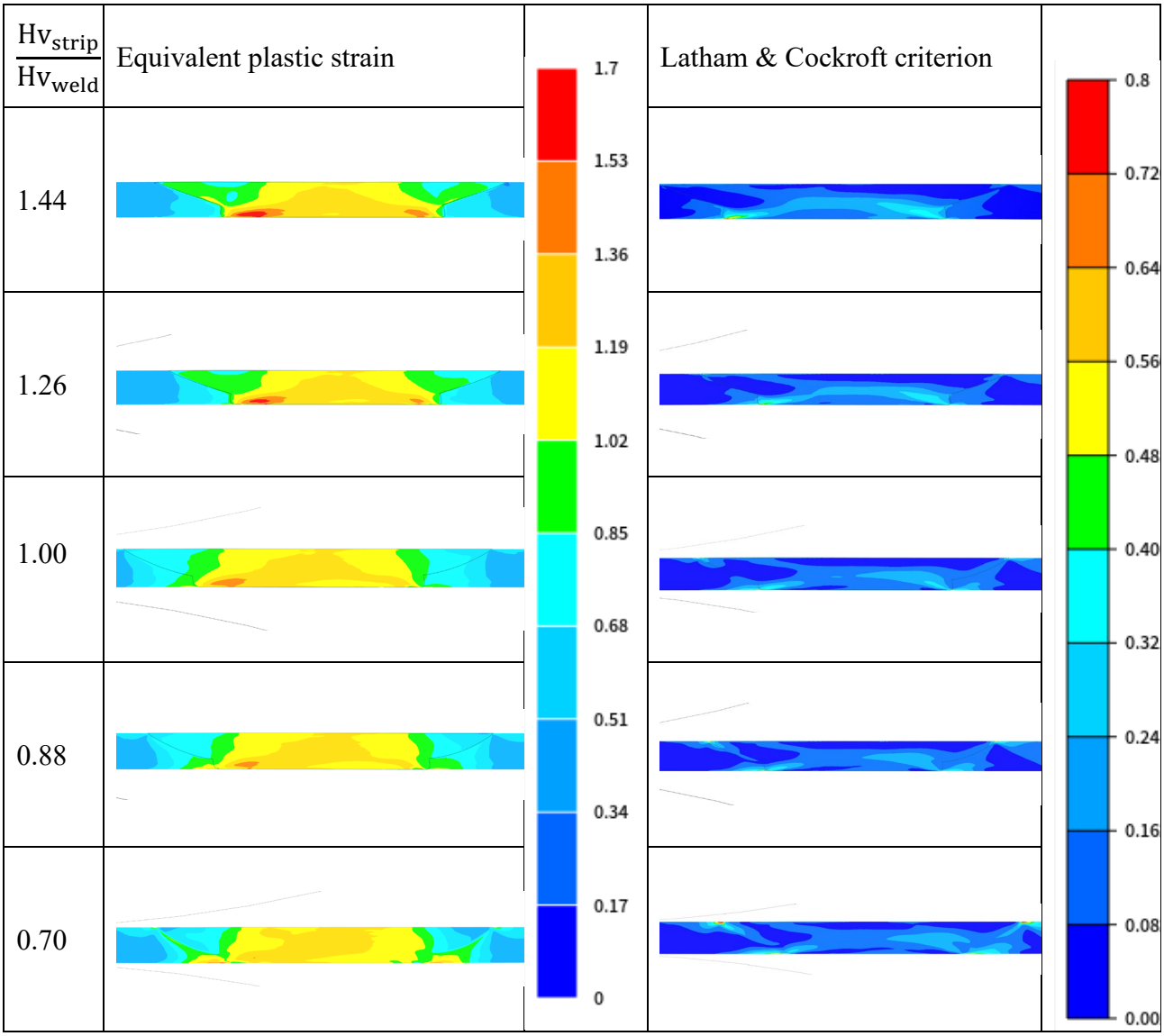

Figure 8: Weld / base metal hardness ratio impact on strain and LC maps (austenitic grades). Rolling direction RD is from left to right.

Scale-breaker. This explanation does not hold however for austenitic grade rolling where the base metal (hot rolled, fine grains) is always harder than the weld metal (solidification microstructure, large grains). The solution lies in this case in through-process defect hunting, including the scale-breaker. Table 1 and Fig. 10 feature the progression of the strip and weld bead through the 3 stands of the scale-breaker, capturing critical instants where the thick, hence rigid bead contacts the rolls in turn and forces the strip to over-bend compared with the steady-state. This results in (1) thinning of the upstream strip next to the weld line, (2) damage.

Table 1: Thickness evolution in the steady state and near the weld line (upstream). Austenitic grade rolling, initial thickness 2.15 mm.

Thickness [mm]	Steady state	Near bead, upstream	Near bead, downstream
After unit 1	2.100	2.088	2.119
After unit 2	2.064	2.046	2.095
After unit 3	2.043	2.007	2.071

Thinning (table 1) occurs mainly on the upstream side. In fact, the downstream side even thickens if compared to the steady state (thinning ~5% brought by simple bending of the strip under tension).

Final values compare well with the near-weld thickness drop measured on the line, 7 to 10% (the latter for ferritic grades). This nourishes confidence in the mechanisms displayed in Fig. 10.

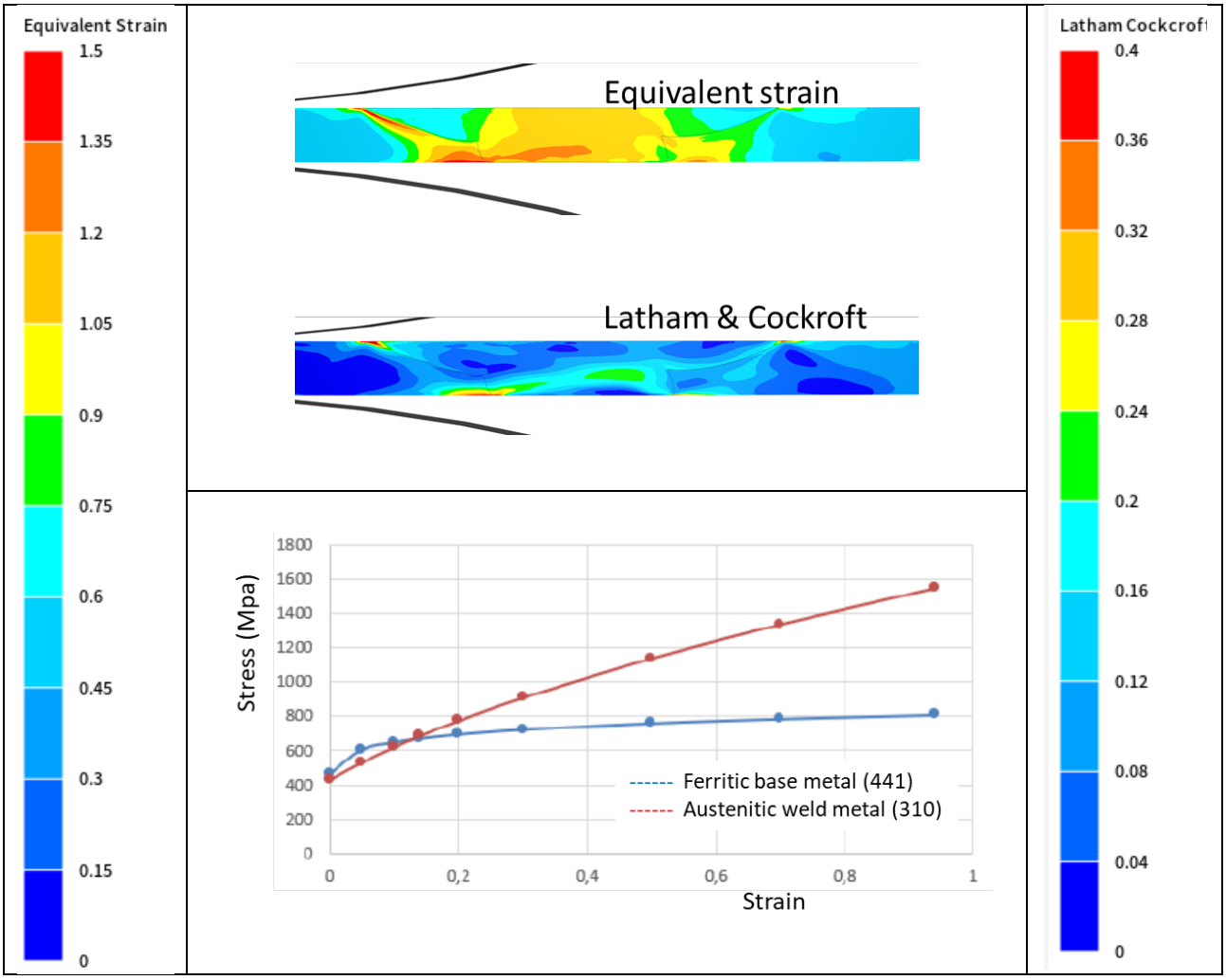

Figure 9: Damage function at the exit of the roll bite, 441 ferritic steel butt-welded using ER 310.

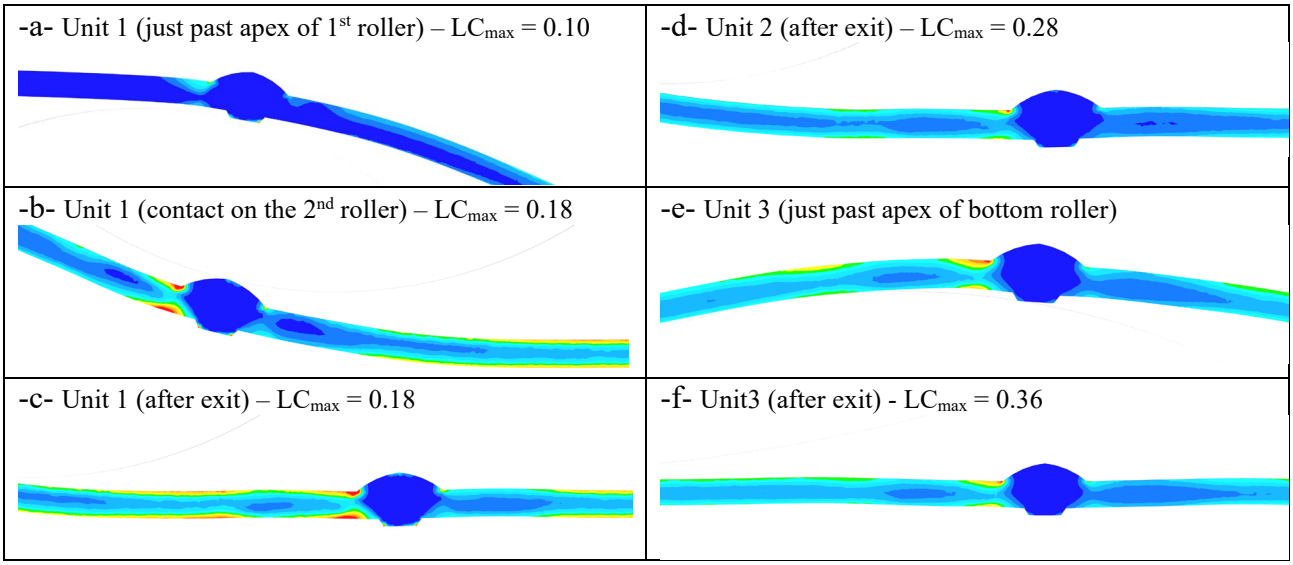

Figure 10: LC damage growth near weld bead as the strip snakes through the 3 scale-breaker units. Strip movement is from left to right.

In all cases, the most damaged point with the largest plastic strain is top upstream. This is due to the way the protruding weld bead, with its high thickness / high stiffness, contacts the rollers and

climbs over them under a high tension. In unit 1 (Fig. 10a-c), as its root (bottom surface) comes in contact, the bead rotates first clockwise, then counterclockwise over the first roller (rotation of the local normal to the strip with respect to the local normal to the roller). This puts the upstream strip top surface in alternating tension and compression, and vice-versa for the bottom surface. The downstream strip undergoes less strain and stress due to the longer free length. Similar events occur in reverse order when the cap of the weld (top surface) contacts the second roller, with more strain and damage since protrusion is bigger. On exit of Unit 1, strain is larger on the upstream side near the bead, quasi-equal on top and bottom surfaces. In Unit 2 (Fig. 10d-e) and further in the "anti-bow" unit (Fig. 10f), the top surface experiences larger strain and thinning, resulting in a damage concentration at the top upstream interfacial point. In the steady state, far from the weld line, thinning is of course uniform whereas strain and damage show the traditional plastic bending pattern. Remember that strain has to be plastic to break the brittle scale.

Overall, largest damage is of the same order at the one incurred in the 1st pass rolling process itself.

Coupled scale-breaker + 1st stand rolling computation. Damage through the scale-breaker being larger at the real position where fracture is observed (top upstream), it might explain this preferred locus when rolling damage is added to scale-breaker damage. This has been investigated by chaining the two operations. Fig. 11 compares LC maps in the non-coupled and coupled cases (austenitic + austenitic, standard conditions). Addition of strain and damage incurred during the two steps now balances damage bottom upstream and top upstream. Due to CPU cost however, a coarser mesh (x3) had to be used for the coupled case, so that only a qualitative conclusion can be drawn at this stage.

-a- LC damage without scale-breaker modelling. Color scale, deep blue to red, stands for [0 … 0.5]

-b- LC damage with scale-breaker modelling. Color scale, deep blue to red, stands for [0 … 0.5]

Figure 11: Strain and damage after scale-breaking and rolling (left to right) of the austenitic grade.

Conclusion

Starting from field observation that stainless steel strip butt-weldings fracture more or less often in the first rolling stand, an approximate model of the operation has been built and simulated by the ForgeNxt® FEM package. Coarse as it may be, the Latham and Cockroft damage approach has yielded, we think, a plausible scenario explaining among others the different fracture frequencies of ferritic (AISI 441) versus austenitic (AISI 304L) grades and the fact that, in spite of technological differences and different deformation mechanisms, both share the same privileged fracture locus.

First, the analysis of the scale-breaking units has shown unexpectedly high plastic strain and damage. This is due to the protrusion of the weld line – a flat strip being bent under tension in the scale-breaker shows plastic strain and thinning but to a non-dangerous extent. The local behavior of the thick and rigid bead, inducing strong over-bending in its vicinity, is the reason why. Of course, this excess of bending strain is all the larger as a thicker bead is formed at butt-welding.

For the ferritic grade, the fact that it is butt-welded with the same austenitic weld metal as the 304L strips is essential: early in the roll bite, the weld metal, with its huge strain-hardening rate, becomes harder than the base metal. It then punches it to the point where an additional shear band forms, bringing high damage. Fracture follows as thickness reduction proceeds in the roll bite. Of course, damage in the scale-breaker adds up and makes things worse. All in all, the addition of these two sources of damage explains why ferritic strips butt-weldings broke quasi-systematically.

For the austenitic grade, the hardness difference is in favor of the base metal. Damage from rolling exists but remains moderate, except if a large weld metal thickness excess occurs – or a strong misalignment of the upstream and downstream strips, also studied but not shown here. Here, the increase of damage by preliminary scale-breaking plays an essential role. Reducing bending amplitude in the scale-breaker could be the solution as tests on the mill have suggested in the past.

The present study has confirmed the importance of risk factors qualitatively pointed out in the scarce technical literature. It has moreover put comparative figures on the risk and shown precise plastic strain and damage mechanisms. On the other hand, several points of interest have been left aside, such as detailed strip and weld metal mechanical and fracture properties, the effect of the HAZ or of plastic heating, all of them potentially bringing the system to critical behavior. This leaves space for future studies and future progress.

References

[1] V.L. Mazur, A.V. Nogovitsyn, Investigation on digital computer of process of continuous rolling of butt-welded strip. Steel in the USSR 10, 10 (1980) 553-555

[2] N.P. Longfield, T.T. Lieshout, E.J. De Wit, Method of producing a continuous metal strip by laser butt welding, with a laser having a multimodal welding power distribution, European Patent 1 870 194 A1 (2007)

[3] E. Dechassey, C. Silvy-Leligois, F. Chicharro Herranz, V. Polo Mestre, M.-C. Theyssier, T. Celotto, C. Kaczynski, T. Dupuy, Q.-T. Ngo, Method for manufacturing cold-rolled, welded steel sheets, and sheets thus produced, US Patent application 20200299796 (2020)

[4] Welders for cold-rolling plants - Primetals Technologies, https://www.primetals.com. Accessed on 11/01/2021

[5] R. Hill, The Mathematical Theory of Plasticity, Oxford University Press (1950), pp. 257 et sq.

[6] L.R. Sanchez, Modeling of springback, strain rate and Bauschinger effects for 2D steady state cyclic flow of sheet metal subjected to bending under tension, Int. J. Mech. Sci. 50 (2010) 429-439

[7] M.G. Cockroft, D.J. Latham, Ductility and the Workability of Metals, J. Inst. Met. 96 (1968) 33–39

[8] Information on https://www.transvalor.com/en/homepage. Accessed on 11/01/2021

[9] K. Mocellin, L. Fourment, T. Coupez, J.L. Chenot, Toward large scale F.E. computation of hot forging process using iterative solvers, parallel computation and multigrid algorithms, Int. J. Num. Meth. Engg. 52 (2001) 473-478

[10] T. Coupez, Parallel adaptive remeshing in 3D moving mesh finite element, in: B.K. Soni, J.F. Thomson, J.H. Vauser, P.R. Eiseman (Eds.), Numerical Grid Generation in Computational Field Simulations, Mississippi State University, Mississippi, USA, 1996, pp. 783–792